University of Reading

Maleimide-functionalised PLGA-PEG nanoparticles as mucoadhesive carriers for intravesical drug delivery

Article

Accepted Version

Creative Commons: Attribution-Noncommercial-No Derivative Works 4.0

Kaldybekov, D., Filippov, S. K., Radulescu, A. and Khutoryanskiy, V. V. ORCID: https://orcid.org/0000-0002-7221-2630 (2019) Maleimide-functionalised PLGA-PEG nanoparticles as mucoadhesive carriers for intravesical drug delivery. European Journal of Pharmaceutics and Biopharmaceutics, 143. pp. 24-34. ISSN 0939-6411 doi: 10.1016/j.ejpb.2019.08.007 Available at https://centaur.reading.ac.uk/85583/

It is advisable to refer to the publisher's version if you intend to cite from the work. See Guidance on citing.

To link to this article DOI: http://dx.doi.org/10.1016/j.ejpb.2019.08.007

Publisher: Elsevier

All outputs in CentAUR are protected by Intellectual Property Rights law, including copyright law. Copyright and IPR is retained by the creators or other copyright holders. Terms and conditions for use of this material are defined in the End User Agreement.

University of Reading

www.reading.ac.uk/centaur

CentAUR

Central Archive at the University of Reading

Reading's research outputs online

Maleimide-functionalised PLGA-PEG nanoparticles as mucoadhesive carriers for intravesical drug delivery

Daulet B. Kaldybekov [a,b], *Sergey K. Filippov* [c], *Aurel Radulescu* [d], *Vitaliy V. Khutoryanskiy* [a,*]

[a] School of Pharmacy, University of Reading, Whiteknights, RG6 6AD Reading, United Kingdom

[b] Department of Chemistry and Chemical Technology, Al-Farabi Kazakh National University, 050040 Almaty, Kazakhstan

[c] Harvard John A. Paulson School of Engineering and Applied Sciences, Harvard University, Cambridge, MA 02138, United States

[d] Forschungszentrum Jülich GmbH, Jülich Centre for Neutron Science (JCNS) at Heinz Maier-Leibnitz Zentrum (MLZ), Lichtenbergstraße 1, 85748 Garching, Germany

*__Corresponding author__

Postal address: School of Pharmacy, University of Reading, Whiteknights, PO Box 224, Reading, RG6 6AD, United Kingdom

E-mail address: v.khutoryanskiy@reading.ac.uk (V.V. Khutoryanskiy)

Phone: +44(0) 118 378 6119

Fax: +44(0) 118 378 4703

Abstract

Low permeability of the urinary bladder epithelium, poor retention of the chemotherapeutic agents due to dilution and periodic urine voiding as well as intermittent catheterisations are the major limitations of intravesical drug delivery used in the treatment of bladder cancer. In this work, maleimide-functionalised poly(lactide-*co*-glycolide)-*block*-poly(ethylene glycol) (PLGA-PEG-Mal) nanoparticles were developed. Their physicochemical characteristics, including morphology, architecture and molecular parameters have been investigated by means of dynamic light scattering, transmission electron microscopy and small-angle neutron scattering techniques. It was established that the size of nanoparticles was dependent on the solvent used in their preparation and molecular weight of PEG, for example, 105 ± 1 nm and 68 ± 1 nm particles were formed from $PLGA_{20K}$-PEG_{5K} in dimethyl sulfoxide and acetone, respectively. PLGA-PEG-Mal nanoparticles were explored as mucoadhesive formulations for drug delivery to the urinary bladder. The retention of fluorescein-loaded nanoparticles on freshly excised lamb bladder mucosa *in vitro* was evaluated and assessed using a flow-through fluorescence technique and Wash Out_{50} (WO_{50}) quantitative method. PLGA-PEG-Mal nanoparticles (NPs) exhibited greater retention on urinary bladder mucosa (WO_{50} = 15 mL) compared to maleimide-free NPs (WO_{50} = 5 mL). The assessment of the biocompatibility of PEG-Mal using the slug mucosal irritation test revealed that these materials are non-irritant to mucosal surfaces.

Keywords: urinary bladder, intravesical drug delivery, PLGA-PEG, maleimide, nanoparticles, small-angle neutron scattering, slug mucosal irritation test, mucoadhesion, Wash Out_{50} (WO_{50}).

1. Introduction

Mucoadhesion can be described as the ability of materials to adhere to mucosal membranes for extended periods of time. Transmucosal drug administration is currently employed in ocular (conjunctival and corneal), nasal, pulmonary, oromucosal (buccal and sublingual), gastrointestinal, rectal, vaginal and intravesical drug delivery, and it offers an alternative to injections [1–6]. Transmucosal drug delivery provides numerous advantages, including (i) prolonged residence time of a dosage form and high density of blood vessels on mucosal surfaces ensure more efficient and rapid drug absorption; (ii) non-oral drug administration allows avoiding its potential degradation in the stomach and prevents hepatic first-pass metabolism; (iii) ease of drug administration and the possibility for quick termination of a therapy resulting in improved patient compliance; (iv) possibility of targeting particular body sites and tissues due to local administration; and (v) reduced administration frequency. Mucoadhesive dosage forms could be highly beneficial for local drug administration to treat posterior segment diseases of the eye [7,8], neurological disorders (*via* intranasal administration) [9,10], and genitourinary tract dysfunctions [11,12].

Intravesical drug delivery (IDD) refers to a direct administration of active pharmaceutical ingredients into the urinary bladder using a catheter inserted through the urethra. This technique is generally used to treat bladder-related disorders, such as bladder cancer (BC) and interstitial cystitis [13–15]. However, the efficiency of this route of drug administration is limited due to dilution and wash out during periodical micturition resulting in poor retention of instilled therapeutic agents. Additionally, the need for frequent catheterisations with potential risks of irritation, inflammatory reactions and infections makes this procedure rather unpleasant for patients [16].

Mucoadhesive materials have the potential to improve the efficacy of IDD by prolonging the drug residence in the bladder. First generation (conventional) mucoadhesive materials are traditionally used as matrixes in many formulations for transmucosal drug delivery. These include hydrophilic polymers of natural and synthetic origin, such as chitosan, carbopols and cellulose derivatives [17–21]. The

adhesion of these macromolecules is due to their ability to interact with glycosylaminoglycans/mucins present on mucosal surfaces through non-covalent interactions such as hydrogen bonding, electrostatic attraction and chain entanglement.

Andreas Bernkop-Schnürch [22] pioneered the use of thiolated polymers (thiomers) as the second generation of mucoadhesives. Well-established water-soluble polymers were modified with thiol functional groups using different chemical approaches to greatly enhance their mucoadhesive properties [23–25]. A few studies reported the use of thiolated mucoadhesives for IDD. For example, thiol-functionalised chitosan nanoparticles have been used for IDD in an *in vitro* study using porcine urinary bladders [26,27]. The ability of these thiolated mucoadhesives to stay adhered on mucosal surfaces is due to the formation of inter-disulphide bridges *via* covalent interaction with cysteine residues present in mucins.

Recently, our group has demonstrated that polymeric nanogels [28] and PEGylated liposomes [29] functionalised with maleimide groups exhibited excellent mucoadhesive properties to bovine conjunctival tissues and freshly excised porcine bladder mucosa, respectively. The ability of these formulations to retain on mucosal tissues, evaluated using a flow-through method, was found to be comparable to a well-known mucoadhesive chitosan. The excellent mucoadhesive performance of these novel advanced formulations is attributed to their ability to form covalent linkages with thiol groups present in the mucus *via* Michael-type addition reactions. Later, other researchers have also reported the development of alginate- and chitosan-based mucoadhesives functionalised with maleimide groups and demonstrated their superior retention/adhesion on/to mucosal surfaces compared to unmodified polysaccharides [30, 31]. All the maleimide-functionalised systems reported so far [28–31] due to their hydrophilic nature were only suitable for formulation of water-soluble drugs. There is also a strong need in the development of mucoadhesive drug delivery systems capable of incorporating poorly-soluble drugs, which will require the use of less polar polymers for their development.

Poly(lactide-*co*-glycolide)-*block*-poly(ethylene glycol) (PLGA-PEG), a block copolymer approved by the US Food and Drug Administration, has been widely employed in controlled release formulations and tissue engineering applications due to its safety, low toxicity, low immunogenicity, high cytocompatibility and biodegradability [32]. PLGA-PEG could easily be self-assembled to micelles or nanoparticles by either simple single emulsion (oil-in-water) or double emulsion solvent evaporation (water/oil/water) techniques [33,34]. For instance, Bazylińska et al. [35] described the influence of preparation parameters, the type of polymer and active cargo on the colloidal and biological stability of final nano-carriers for further *in vitro* and *in vivo* applications. Pei et al. developed the application of pH-sensitive intravenous PLGA-PEG formulations to deliver vancomycin in the therapy against intracellular pathogens [36]. PLGA-PEG nanoparticles functionalised with maleimide groups were also recently reported as carriers for drug delivery. Their maleimide-functionalised surface was used for further modification with monoclonal antibody [37] and cell penetrating peptides [38].

In the present work, we report the design of maleimide-functionalised PLGA-PEG nanoparticles as potential mucoadhesive formulations for IDD to urinary bladder and demonstrate that surface maleimide groups could significantly enhance mucoadhesive properties of these materials. Four types of nanoparticles were developed using PLGA-PEG containing 3 and 5 kDa PEG with and without maleimide terminal groups. The structural features of these nanoparticles were studied using small-angle neutron scattering, dynamic light scattering and transmission electron microscopy. The hydrophobic nature of PLGA-based core of the nanoparticles provided an excellent opportunity for formulating poorly water-soluble compound as a model drug. These nanoparticles were loaded with lipophilic fluorescein and their retention on urinary bladder mucosa was studied *in vitro*. Slug mucosal irritation *in vivo* test was used to assess the biocompatibility of PEG-Mal present on the surface of these nanoparticles.

2. Materials and methods

2.1. Materials

Four different di-block copolymers of poly(lactide-*co*-glycolide)-poly(ethylene glycol) ((methoxy-terminated: Mw 20,000 : 3,000 Da, PDI 1.30 ($PLGA_{20K}$-PEG_{3K}) and Mw 20,000 : 5,000 Da, PDI 1.65 ($PLGA_{20K}$-PEG_{5K}); maleimide-functionalised: Mw 20,000 : 3,400 Da, PDI 2.70 ($PLGA_{20K}$-PEG_{3K}-Mal) and Mw 20,000 : 5,000 Da, PDI 2.42 ($PLGA_{20K}$-PEG_{5K}-Mal)) were purchased from PolySciTech® Akina Inc. (West Lafayette, IN, USA; catalogue numbers: AK101, AK037, AI109, AI020). Dimethyl sulfoxide (DMSO) was purchased from Fisher Scientific (Loughborough, UK), acetone and deuterium oxide (D_2O), benzalkonium chloride (BAC), poly(ethylene glycol) methyl ether (PEG; average Mn 5,000 Da), methoxypolyethylene glycol maleimide (PEG-Mal; average Mn 5,000 Da) and phosphate buffered saline tablets (PBS) were purchased from Sigma-Aldrich (Gillingham, UK). 6-Maleimidohexanoic acid was purchased from Alfa Aesar (Heysham, UK). Fluorescein was purchased from Acros Organics (Geel, Belgium). All other chemicals were of analytical grade and used as received.

2.2. Preparation of nanoparticles

Empty and fluorescein-loaded PLGA-PEG nanoparticles were prepared *via* one-step nanoprecipitation (single emulsion) technique followed by dialysis. In brief, 20 mg of polymers and 1 mg fluorescein were dissolved in 1 mL of DMSO or acetone to form organic phase. The organic phase was then added to 30 mL of deionised water dropwise under constant stirring to form a colloidal suspension, which was allowed to stir gently for 1 h. Finally, this suspension was purified by dialysis against deionised water (5L; 4 changes) using a dialysis membrane tube (molecular weight cut-off 12–14 kDa; Medicell Membranes Ltd., UK) to remove residual solvent, filtered using 0.22 µm Minisart® syringe filters and stored in a fridge for further use.

2.3. Particle size and zeta potential analysis

The size of fluorescein-free PLGA-PEG nanoparticles, their polydispersity index (PDI) and zeta-potential values were determined using dynamic light scattering (DLS) at a scattering angle of 173° with a Zetasizer Nano-NS (Malvern Instruments, UK). Each nanoparticle dispersion was diluted 100-fold with ultra-purified water. Refractive index of 1.59 and absorbance of 0.01 were used in all measurements. Each sample was analysed three times at 25 °C and the Z-average mean ± standard deviation values were calculated.

2.4. Transmission electron microscopy (TEM)

Nanoparticles were imaged using a JEOL 2100 Plus TEM operated at an acceleration voltage of 200 kV. Specimens were prepared by pipetting a drop of purified nanoparticle suspension (about 0.5 mg/mL) onto a parafilm. A glow-discharged holey carbon film-coated 400-mesh copper grid was then placed onto the drop with "carbon" side and left in contact with the sample for 60 sec. The excess solution was removed by blotting with a filter paper. Then, a drop of 2% (w/v) uranyl acetate (UA) solution was deposited onto the parafilm and the grid remained in contact with "carbon" side with UA for another 60 sec. The excess stain was removed by dabbing similarly as above and the sample was left to dry in air prior to TEM characterisation. This sample preparation technique was previously reported to give good quality of images for PLGA-PEG nanoparticles [39].

2.5. Small-Angle Neutron Scattering (SANS) study

PLGA-PEG nanoparticles were prepared as described above. Briefly, 10 mg of polymers were dissolved in 1 mL of organic solvent (acetone or DMSO). This solution was then added to 20 mL of D_2O dropwise under continuous stirring to form suspension of nanoparticles, which was then allowed to stir gently for an additional 20 min. Finally, 2 mL of aliquot was aspirated from the suspension and dialysed using a Spectra-Por® Float-A-lyzer® G2 dialysis membrane, with a molecular weight cut-off 3.5–5 kDa, against D_2O to remove residual solvent, filtered using 0.22 µm Minisart® syringe filters and stored in a fridge prior to SANS studies.

SANS experiments were performed at MLZ (Garching, Germany) on KWS-2 instrument [40]. Measurements were made on a ^{3}He tubes array detector (144 tubes, pixel size 8 mm) using a non-polarised, monochromatic (wavelength λ set by a velocity selector) incident neutron beam collimated with rectangular apertures for two sample-to-detector distances, namely 2, 8, and 20 m ($\lambda = 0.6$ nm). With this setup, the investigated q-range was 0.015 nm^{-1} to 4.6 nm^{-1}. In all cases, the two-dimensional scattering patterns were isotropic and were azimuthally averaged, resulting in the dependence of the scattered intensity $I_s(q)$ on the momentum transfer $q = 4\pi sin\theta/\lambda$, where 2θ is the scattering angle. The curves were corrected for background scattering from the empty cell and for detector efficiency. Hellma® Analytics Suprasil® 300 high precision quartz cells of 1 and 2 mm thickness were used for experiments. SANS experiments were performed in D_2O solution. The D_2O solution was measured and properly subtracted. The concentration of nanoparticles used in SANS measurements was 0.5 mg/mL.

2.6. SANS data fitting

The scattered intensity curves were fitted using the model of sphere with attached Gaussian chain having self-avoiding walk statistics implemented in SASFit software [41] based on the model developed by Pedersen et al. [42] (Fig. 1).

The scattering curves in D_2O could be fitted using the following function:

$$I(q) = P_{sgc}(q)S(q) \quad (1)$$

We assume that $S(q) = 1$ due to low concentration of nanoparticles in solution, 1 mg/mL. The overall scattering intensity of the sphere with attached Gaussian chain written as:

$$P_{sgc} = N_{agg}^2\beta_{core}^2P_{core}(q) + N_{agg}\beta_{brush}^2P_{brush}(q) + 2N_{agg}^2\beta_{core}\beta_{brush}S_{brush-core}(q) + N_{agg}(N_{agg} - 1)\beta_{brush}^2S_{brush-brush}(q) \quad (2)$$

where $N_{agg}^2\beta_{core}^2P_{core}(q)$ is self-correlation term of the core; $N_{agg}\beta_{brush}^2P_{brush}(q)$ is self-correlation term of the chains; $2N_{agg}^2\beta_{core}\beta_{brush}S_{brush-core}(q)$ is the cross-term between the core and chains and $N_{agg}(N_{agg}-1)\beta_{brush}^2S_{brush-brush}(q)$ is the cross-term between different chains. N_{agg} is the aggregation number of polymers forming the nanoparticle per surface area, $\beta_{brush}=V_{brush}(\eta_{brush}-\eta_{solv})$ and $\beta_{core}=V_{core}(\eta_{core}-\eta_{solv})$ are the excess scattering lengths of a block in the corona and in the core, respectively. V_{brush} and V_{core} are the total volume of a block in the corona and in the core, respectively. η_{brush} and η_{core} are the corresponding scattering length densities (SLDs). $P_{core}(q)$ is scattering of spherical core

$$P_{core}(q,R_{core})=3\frac{(\sin(qR_{core})-qR_{core}cos(qR_{core}))}{(qR_{core})^3} \quad (3)$$

The scattering intensity for the brush is given by:

$$P_{brush}\left(q,R_{gchain}\right)=2\frac{exp(-x)-1+x}{x^2} \quad (4)$$

where $x=R_{gchain}^2q^2$; R_{gchain} is the gyration radius of a polymer chain.

The contribution of cross term between core and chains which form brush of wormlike micelle is calculated using equation:

$$S_{brush-core}\left(q,R_{core},R_{gchain},d\right)=\psi\left(qR_{gchain}\right)P_{core}(q,R_{core})\frac{sin(q[R_{core}+dR_{gchain}])}{q[R_{core}+dR_{gchain}]} \quad (5)$$

where $\psi\left(qR_{gchain}\right)=\frac{1-exp(-x)}{x}$ is the form factor amplitude of the chain.

The contribution of cross term between chains is calculated using equation:

$$S_{brush-brush}\left(q,R_{core},R_{gchain},d\right)=\psi^2\left(qR_{gchain}\right)\left[\frac{sin(q[R_{core}+dR_{gchain}])}{q[R_{core}+dR_{gchain}]}\right]^2 \quad (6)$$

where d is parameter that accounts for non-penetration of the chains into the core and should be mimicked by $d \sim 1$ for $R_{core} \gg R_{gchain}$.

The model has the following fitting parameters: R_{core} – core radius; V_{core} – molecular volume of single block unit in the micellar core; V_{brush} – molecular volume of single block unit in the micellar corona; η_{core} – scattering length density of spherical core; η_{brush} – scattering length density of the block unit in the corona; η_{solv} – scattering length density of solvent; R_{gchain} – gyration radius of polymer chains in the corona; L – contour length of polymer chain, b – Kuhn segment length.

Excess scattering lengths of solvent and polymeric shell, V_{core}, V_{brush}, contour length of polymer chain, Kuhn segment length were known from literature data and polymer composition and were chosen to be fixed during the fitting procedure.

To account for nanoparticles polydispersity, a Schulz-Zimm distribution of R_{core} with polydispersity parameter σ was included in the following way:

$$SZ = \frac{R_{core}^{Z}}{\Gamma(Z+1)}\left(\frac{Z+1}{<R_{core}>}\right)^{Z+1} exp\left[-\frac{(Z+1)R_{core}}{<R_{core}>}\right] \quad (7)$$

where $Z = \frac{1}{\sigma^2} - 1$ (8)

The gyration radius R_g of nanoparticles was calculated from Guinier regime to evaluate the overall size of nanoparticles.

2.7. Encapsulation efficiency and loading capacity

Amicon® Ultra-0.5 Ultracel-3 centrifugal filter unit with a molecular weight cut-off 10 kDa was used in these experiments. Each centrifugal filter device was pre-rinsed with PBS (500 µL) at 13,000 rpm (7558 × g) for 30 min prior to further use. The dispersion of PLGA-PEG nanoparticles (500 µL) was placed in an ultrafiltration tube and centrifuged at 4 °C at 13,000 rpm (7558 × g) for 30 min. This loading

step was repeated twice. The filtrate was discarded and the retentate was washed with 250 μL of PBS by further centrifugation at 4 °C at 13,000 rpm (7558 × g) for 20 min. The filtrate was withdrawn again and the fluorescein-loaded PLGA-PEG nanoparticles in the retentate were then mixed with 100 μL DMSO (left for 6 h in a fridge to dissolve the nanoparticles and model drug) and spun at 4 °C at 13,000 rpm (7558 × g) for 10 min. The amount of free fluorescein in the supernatant was quantified using a Varian Cary Eclipse fluorescence spectrophotometer at $\lambda_{excitation}$ and $\lambda_{emission}$ = 460 and 513 nm, respectively, and the encapsulation efficiency (EE%) and loading capacity (LC%) were determined using the following formulae:

$$EE\% = \frac{C}{C_i} \times 100 \quad (9)$$

$$LC\% = \frac{C}{Total\ weight\ of\ NPs} \times 100 \quad (10)$$

where C is the amount of fluorescein encapsulated in the nanoparticles (NPs), and C_i is the initial amount of fluorescein. A standard curve was generated by plotting the fluorescence intensities from different concentrations of the model drug and used to calculate EE% and LC% can be found in Supplementary Information (Fig. S1).

2.8. Toxicology: slug mucosal irritation test

The slug mucosal irritation test (SMIT) was carried out according to our previously published report [43]. *Arion lusitanicus* slugs were collected locally in Harris Garden (Reading, UK) and were housed in specially designed plastic containers and fed with lettuce, cabbage, carrots and cucumber. Each slug's body lining was carefully examined and only slugs showing no evidence of macroscopic injuries with clear tubercles and a foot surface were used for testing purposes. Slugs weighing between 15 and 23 g were isolated from the culture and were kept individually in 1.5 L glass beakers lined with a paper

towel soaked with 20 mL of PBS solution and left at room temperature for 48 h before the start of an experiment. All beakers were covered with a cling film pierced with tiny holes in order to allow air exchange. Each slug was individually weighed before the experiment and then placed in 90 mm Petri dishes lined with Whatman™ filter paper moistened with either positive/negative controls (2 mL of 1% BAC prepared in PBS and 2 mL of PBS solution, respectively) or 2 mL of each test materials (PEG, PEG-Mal and MHA) with the following concentrations: 0.00003; 0.0003; 0.003 and 0.03 mmol prepared in PBS. After 60 min contact period slugs were taken out, rinsed with 10 mL of PBS, gently wiped with the paper towel and then reweighed. The percentage of mucus production (MP%) was estimated as a slug body weight loss and evaluated using the following equation:

$$MP\% = \frac{(m_b - m_a)}{m_b} \times 100 \quad (11)$$

where m_b and m_a are the weights of a slug before and after experiment, respectively. Each experiment was repeated 7 times using different slugs and the results were evaluated statistically, calculating the mean ± standard deviation values.

2.9. Preparation of artificial urine solution

Artificial urine solution was prepared according to the previously reported protocol [44]. Briefly, the following components were dissolved in deionised water by stirring overnight at room temperature, before making the total volume to 2000 mL: urea (24.27 g), uric acid (0.34 g), creatinine (0.90 g), sodium citrate dihydrate ($Na_3C_6H_5O_7 \cdot 2H_2O$, 2.97 g), sodium chloride (NaCl, 6.34 g), potassium chloride (KCl, 4.50 g), ammonium chloride (NH_4Cl, 1.61 g), calcium chloride dihydrate ($CaCl_2 \cdot 2H_2O$, 0.89 g), magnesium sulfate heptahydrate ($MgSO_4 \cdot 7H_2O$, 1.00 g), sodium bicarbonate ($NaHCO_3$, 0.34 g), sodium oxalate ($Na_2C_2O_4$, 0.03 g), sodium sulphate (Na_2SO_4, 2.58 g), sodium phosphate monobasic monohydrate

258 ($NaH_2PO_4 \cdot H_2O$, 1.00 g), and sodium phosphate dibasic (Na_2HPO_4, 0.11 g). The artificial urine solution
259 (pH 6.40) was kept at 37 °C throughout the experiments.

260 **2.10. *In vitro* retention studies on lamb urinary bladder mucosa**

261 The retention of PLGA-PEG nanoparticles on lamb urinary bladder tissues *in vitro* was determined
262 using a protocol previously described by our group with minor modifications [29]. Lamb bladder tissues
263 were received from P.C. Turner Abattoirs (Farnborough, UK) immediately after animal slaughter,
264 packed, frozen and transported in an insulated plastic container. The tissues were subsequently thawed
265 upon arrival and carefully excised to yield approximately 2 × 3 cm sections, avoiding contact with the
266 internal mucosa, which were then used in the experiments. The dissected bladder tissue was mounted on
267 a glass slide with mucosal side facing upward and rinsed with 3 mL of artificial urine (AU; pH 6.40)
268 solution. Experiments were performed with the bladder tissues maintained at 37 °C in an incubator.
269 Aliquots (200 µL) from fluorescein-loaded PLGA-PEG nanoparticle stock solutions were withdrawn and
270 deposited onto a mucosal surface and rinsed with AU at a constant flow rate of 2 mL/min using a syringe
271 pump (total washing time was 50 min). Fluorescence images of a bladder tissue were taken using Leica
272 MZ10F stereo-microscope (Leica Microsystems, UK) with Leica DFC3000G digital camera at 1.6×
273 magnification with 30 ms exposure time (gain 2.0×), fitted with a GFP filter. The microscopy images
274 were then analysed with ImageJ software by measuring the pixel intensity after each irrigation with AU.
275 The pixel intensity of the blank samples (bladder mucosa without test material) were subtracted from
276 each measurement and data are converted into numbers. All measurements were conducted in triplicate.
277 Evaluation of formulations retention on the mucosa *in vitro* was quantified through WO_{50} values,
278 which represent the volume of a biological fluid necessary to wash out 50 % of a mucoadhesive excipient
279 from a substrate [45]. WO_{50} values of test materials were calculated *via* extrapolation of the average
280 wash-off profiles to 50% using polynomial fitting (5th order) and Wolfram Alpha (a computational
281 knowledge engine).

2.11. Statistical analysis

Statistical analysis of data, i.e. mean values ± standard deviations were calculated and assessed for significance using two-tailed Student's *t*-test and a one-way analysis of variance (ANOVA) followed by Bonferoni *post hoc* test using GraphPad Prism software (version 7.0), where $p < 0.05$ was fixed as the statistical significance criterion.

3. Results and discussion

3.1. Preparation and characterisation of nanoparticles

PLGA-PEG nanoparticles, with and without fluorescein, were formulated using single emulsion method and precipitated from acetone and DMSO. The detailed preparation procedure of nanoparticles is illustrated in Fig. 2. The average mean diameter of all PLGA-PEG nanoparticles precipitated from DMSO remained ~100 ± 1 nm on average regardless of the molecular weight of PEG moiety in block copolymers, whereas the nanoparticles precipitated from acetone displayed smaller values of 65 ± 1 nm and 80 ± 1 nm for PLGA-PEG and PLGA-PEG-Mal, respectively. We believe that the difference in the particle sizes might depend on the dielectric constant of organic solvent (acetone, $\varepsilon = 21$ and DMSO, $\varepsilon = 47$) and their miscibility with water during formation of nanoparticles in aqueous phase [46]. It is also interesting to compare our results with the study reported by Yang et al. [47], who prepared PLGA-PEG nanoparticles from acetone, acetonitrile and tetrahydrofuran. They reported the solvent effect on the particle size with formation of 154 ± 3, 134 ± 2 and 186 ± 4 nm of nanoparticles from acetone, acetonitrile and tetrahydrofuran, respectively. Our nanoparticles prepared from acetone are much smaller (65 ± 1 nm), which shows the strong influence of other factors, including individual block molecular weights and particle preparation techniques.

All nanoparticles prepared in the present study showed negative zeta-potential greater than –21 mV and had low polydispersity of less than 0.20, indicating the presence of a homogeneous population with

a narrow size distribution (Fig. 3). The physicochemical characteristics of PLGA-PEG nanoparticles are summarised in Table 1.

Fluorescein was used as a model drug to demonstrate the potential application of PLGA-PEG nanoparticles in drug delivery to urinary bladder. Fluorescein (partition coefficient, logP = 3.35, [48]) was loaded into the nanoparticles by first preparing the model drug solution in the organic solvent followed by dissolution of polymers and further nanoprecipitation in deionised water.

The size and morphology of nanoparticles were further confirmed by TEM analysis and microphotographs are displayed in Fig. 4. Uranyl acetate was used as a negative staining to achieve reasonable contrast. TEM analysis revealed the formation of homogeneous vehicles with well-dispersed spherically shaped core and shell structure of nanoparticles and the results are in good agreement with the data obtained by DLS measurements (Table 1).

3.2. Nanoparticle structure

Small-angle neutron scattering (SANS) was used to probe the nanoparticle architecture and determine their molecular parameters. The use of SANS allows to get more information about small particles compared to DLS method. The scattering intensity $I(q)$ curves for all nanoparticle solutions are presented in Fig. 5A and 5B. Several issues should be noted from the inspection of these scattering curves. First, all curves have monotonous behaviour with q; no additional maxima are observed. It is a typical manifestation of moderate or high polydispersity for compact objects. Second, all curves are similar in the middle and high q ranges that implies similarity of all nanoparticles from inside disregarding preparation way and used solvent. The only difference between the scattering curves is visible in low q range that is probably related to the difference in the aggregation number. To have a deeper information, the gyration radius values of nanoparticles in solution were calculated using Guinier approximation (Table 2). Comparison of gyration and hydrodynamic radii reveals that these two parameters are clearly correlated. In agreement with DLS data, the gyration radius value for PLGA-PEG

329 and PLGA-PEG-Mal nanoparticles precipitated from DMSO is nearly the same and insensitive to the
330 PEG molecular weight to the presence of maleimide groups (Table 2). In contrast, the gyration radius
331 value of nanoparticles precipitated from acetone is higher for longer length of a PEG chain. The ratio of
332 gyration and hydrodynamic radii R_g/R_h have been known as the ρ parameter that is sensitive to the
333 architecture of nano-objects. It provides model-independent clue on spatial arrangement of a scattering
334 object [49–53], its theoretical value is known for some simple models such as a hard sphere ($\rho =$
335 0.775), Gaussian chain in Θ-solvent ($\rho = 1.5$), long rods ($\rho > 2.0$). The ρ parameter value calculated
336 for PLGA-PEG and PLGA-PEG-Mal nanoparticles precipitated from DMSO undoubtedly pointing out
337 on a spherical symmetry and compact structure in agreement with TEM results presented above. The
338 change from DMSO to acetone results in the formation of nanoparticles with more loose structure since
339 they have higher ρ parameter value. Increasing of PEG molecular weight leads to increase in ρ value
340 highlighting the enhanced branching structure for 5 kDa PEG nanoparticles made from acetone. We have
341 to mention here that some of these systems have ρ value that is below the lowest possible theoretical
342 limit, 0.775. Nevertheless, low values were already reported in a variety of publications. The ρ parameter
343 fluctuates around 0.8, an average value for all types of nanoparticles justifying the choice of the fitting
344 model described in Experimental Section.

345 The scattering curves obtained for the D_2O solutions can be well fitted with the "sphere with
346 attached Gaussian chain having self-avoiding walk statistics" model, assuming a Schulz-Zimm
347 distribution for core radius. The calculated structural parameters are presented in Table 2.

348 The obtained value of the core radii and shell thickness are in the range of 12–24 nm, which is in
349 agreement with the R_h as observed in the DLS measurements and TEM. In all series of nanoparticles
350 prepared by precipitation from acetone and DMSO, R_{gchain} increases with increase in PEG molecular
351 weight (Table 2), whereas R_{core} is much less sensitive to PEG chain length.

Our results corroborate with SANS studies of PLGA-PEG based block copolymers published previously [47,54–57] keeping in mind the difference in composition, molecular weights and methods of preparation. For example, PEO-PLGA-PEO [55] and PLGA-PEG-PLGA [56] triblock copolymers were investigated using SANS. Apart from the difference in composition, triblock *vs* diblock, the copolymers reported in these papers were different on other important aspects. The molecular weight, Mn, of PLGA block was much lower than the one in our case, 3,500 g/moL [55] and 1,170 g/moL [56], respectively. In both cases solutions were prepared by direct dissolving in D_2O in contrast with solvent exchange method exploited in the present paper. Additionally, structure factor was involved in the fitting procedure since the triblock copolymer solution were in semi-diluted regime, 24 and 20 wt.% for PEO-PLGA-PEO and PLGA-PEG-PLGA, respectively. Applying the Percus-Yevick (PY) hard-sphere model to describe the structure factor and Global Indirect Fourier Transformation (GIFT) to describe the form factor of the micelles composed of PEO-PLGA-PEO at 30 °C, the authors obtained the following values for the radii of a core and shell, 5.9 and 2.5 nm, respectively [55]. The presence of a shell was also reported by Khorshid et al for flower-like micelles composed by PLGA-PEG-PLGA triblock copolymers [56]. SANS method successfully disseminates the internal structure of nanoparticles. The SANS experiments give a clear evidence of asymmetric ellipsoid nanoparticles for the copolymer with the PEG block (Mn = 1,000 g/moL), whereas spherical micelles with core-shell topology is observed for the polymer with longer PEG central block (Mn = 1,500 g/moL). The core-shell cylinder and spherical shell models were utilised to fit the SANS data [56]. Unlike the PEO-PLGA-PEO system, both PLGA-PEG-PLGA copolymers were studied not only in semi-diluted but also for diluted concentration, 1 wt.%. The core and shell radii for $PLGA_{1170}$-PEG_{1500}-$PLGA_{1170}$ were 5.0 nm and these values are much lower in comparison with the data reported in our manuscript, R_{core} and R_{gchain}, Table 2, that is not surprising keeping in mind much higher molecular weights for PLGA and PEG of our copolymers.

Interesting contrast variation SANS study was performed for laponite/PEG1.0k-PLGA0.8k and laponite/PEG1.0k-PLGA1.6k nanocomposites in a broad range of D_2O/H_2O mixture concentrations [57].

It was found that for 66 % of D_2O, the scattering from laponite is matched to the scattering of solvent. The combination of core-shell spherical model in combination with Debay form factor was used for the fitting the scattering profile from laponite free nanoparticles made of PEG-PLGA copolymers. The radius of a core and the micelles was found 1.6 and 4.7 nm, respectively, giving the shell thickness value to be of 3.1 nm [57]. We note here that the model used in our work is very close to the one reported in [57]. Two SANS studies that are the most relevant to our paper deal with nanoparticles composed from PLGA-PEG [47] and PLA-PEG [54] diblock copolymers. In both papers, nanoparticles were prepared by solvent exchange method. The spherical model with a polydisperse core of constant scattering density and diffusive shell was applied for the fitting of PLA-PEG copolymers [54]. The fitting data reported for the acetone as the organic solvent and copolymer with similar composition PLA_{15600}-PEG_{5000} are in perfect agreement with our results for $PLGA_{20K}$-PEG_{5K} (Table 2). The mean core radius of the nanoparticles made of PLA_{15600}-PEG_{5000} is 11 nm, which correlates with our results, 12 nm. The Schultz-Zimm poldispersity values are almost identical, 0.27 [54] *vs* 0.21 in our study. The thickness of the PEG shell of 6.7 nm for PLA_{15600}-PEG_{5000} also agrees well with our data for $PLGA_{20K}$-PEG_{5K} that was found to be 6.9 nm.

Surprisingly, the similar systems measured recently show clearly distinctive results [47]. The PLGA-PEG nanoparticles prepared by solvent exchange method presumably composed from micelles that form a fractal structure inside of a nanoparticle. One of the plausible explanations could be the existence of some residual reactive groups on PLGA-PEG copolymers reported in [47]. Such reactive groups might form bridges between PLGA-PEG micelles.

The choice of the solvent used for precipitation has the greatest impact on nanoparticles structure. Interestingly, nanoparticles dissolved and precipitated from acetone have not only a smaller core but also lower R_{gchain} value in comparison with the NPs precipitated from DMSO. This is a rather unpredicted result that might indicate a different local structure of the interface between PLGA core and PEG brush and different conformation of PEG chains. Indeed, the gyration radius of a PEG chain is twice lower for

NPs precipitated from acetone. Such striking difference could only be explained by compaction of PEG chains on the surface of nanoparticles precipitated from acetone and, in reverse, fully stretched PEG conformation in case of NPs made from DMSO. This hypothesis is indirectly supported by another peculiar feature observed from the SANS results fitting: the presence of maleimide terminal groups increases the R_{gchain} for DMSO series, and in reverse, decreases R_{gchain} for NPs precipitated from acetone (Table 2). We hypothesize that NPs prepared from DMSO have a narrow interface between PLGA and PEG blocks, whereas precipitation from acetone somehow facilitates the formation of the broad interface layer where PLGA and PEG coexist. Inevitably, bulky maleimide groups attached to the dangling PEG chains increase the gyration radius of PEG for NPs precipitated from DMSO. For NPs precipitated from acetone we might expect that some of Mal groups, due to hydrophobic nature of maleimide, will have tendency to incorporate into smooth PLGA-PEG interface (see inserts in Fig. 5). Provided that the nanoparticles precipitated from DMSO have the greatest presence of active maleimide groups on their surface, all subsequent experiments were performed with these samples.

3.3. Mucosal irritancy

The information about the biocompatibility and toxicological characteristics of maleimide-containing materials is currently lacking in the literature. Previously, the biocompatibility of polysaccharides functionalised with maleimide groups was evaluated only by Shtenberg et al. [30] using normal human dermal fibroblasts and by Sahatsapan et al. [31] using human gingival fibroblast cells.

The slug mucosal irritation test (SMIT) was developed by Adriaens et al. [58,59] to evaluate the mucosal irritancy potential of different formulations and active ingredients. It uses terrestrial slug species, which are considered to have limited sentience and so are not protected by regulations covering animal experiments [58]. Normally, slugs release mucus to aid their locomotion. They also produce mucus and lose body weight when in contact with irritating substrates. When their mucosal tissue is damaged the slugs release additional proteins and enzymes. This indication allows for quantifiable outcomes as for

426 irritants to be classified as non-irritating, mild or severely irritating. Generally, mild irritants cause an
427 increase in mucus production, whereas severe irritants result in tissue erosion and more mucus release in
428 addition to increased production [60].

429 Previously we reported the use of SMIT for assessing mucosal irritancy of 2-
430 hydroxyethylmethacrylate and 2-hydroxyethylacrylate based random copolymers of different
431 compositions as well as blend films based on poly(acrylic acid) and methylcellulose using *Limax flavus*
432 and *Arion lusitanicus* slugs [43,61]. In the present work, we have adopted the same methodology and
433 used *Arion lusitanicus* slugs to evaluate the ability of model compounds PEG, PEG-Mal and 6-
434 maleimidohexanoic acid (MHA) to cause mucosal irritation. Fig. 6 presents the results on mucus
435 production by slugs exposed to filter paper surfaces moistened with solutions of PEG, PEG-Mal and
436 MHA of various concentrations prepared in PBS as well as positive and negative controls. In experiments
437 with 1% solution of BAC in PBS (pH 7.50), used as a positive control, slugs experienced a severe
438 discomfort, producing approximately 38 ± 7% of yellow mucus, whereas slugs exposed to PBS (used as
439 a negative control, pH 7.74) did show a low level of mucus production of 5 ± 1%. These data are in good
440 agreement with our previous studies [43,61]. A significant variability of the data obtained from
441 experiments with positive control is explained by slugs' increased activity and tendency to escape a
442 contact with an irritant chemical. In all experiments with negative control and polymeric excipients slugs
443 secreted colourless mucus, which is the first demonstration of their reasonably good biocompatibility.

444 The concentration of test materials of 0.0003 mmol, used to prepare PLGA-PEG nanoparticles in
445 dispersion, was chosen as a reference for the preparation of liquid formulations with model maleimide-
446 containing compounds (MHA and PEG-Mal). Filter paper soaked with 0.03 mmol MHA (pH 4.34)
447 displayed significantly higher irritancy ($p < 0.001$) compared to PEG-Mal (0.03 mmol; MP 6 ± 2%; pH
448 6.92) with the level of mucus production reaching 21 ± 7% and confirming the ability of MHA to irritate
449 mucosal epithelia due to, mainly, its acidic nature (Fig. 6). Additionally, slugs exposed to positive control
450 exhibited an extreme discomfort ($p < 0.0001$) compared to slugs in response to contact with 0.0003 mmol

PEG-Mal. However, filter paper soaked with increasing concentrations of PEG and PEG-Mal demonstrated low irritation potential as no significant differences ($p > 0.5$) were observed between these materials and the negative control. Fig. S2 and Fig. S3 in Supplementary Information provide the detailed schematic illustration of SMIT test and the photographs of mucus production by *Arion lusitanicus* slugs exposed to various test chemicals, respectively. Safety, non-toxicity, and biocompatibility of PEG-Mal allows us to conclude that PLGA-PEG-Mal nanoparticles should not cause irritation in the bladder lining. The non-irritant nature of maleimide-functionalised materials established in this study is also in good agreement with the data reported by Shtenberg et al. [30], who reported that alginate modified with maleimide-terminated PEG is non-toxic to normal human dermal fibroblasts. The maleimide-functionalised chitosan was also reported by Sahatsapan et al. [31] to be non-toxic to gingival fibroblast cells (HGF) up to 1000 μg/mL of polymer in solution.

3.4. Mucoadhesion studies

The retention properties of fluorescein-loaded PLGA-PEG and PLGA-PEG-Mal nanoparticles on lamb urinary bladder mucosa were evaluated using a flow-through method with fluorescent detection using the methodology described in our previously published paper [29]. Fig. 7 shows exemplary fluorescent images of the retention of PLGA-PEG and PLGA-PEG-Mal nanoparticle dispersions on urinary bladder mucosa irrigated with AU. After analysis of the fluorescent images using ImageJ software, it was established that maleimide-functionalised $PLGA_{20K}$-PEG_{5K}-Mal and $PLGA_{20K}$-PEG_{3K}-Mal nanoparticles exhibited greater mucoadhesive properties compared to unmodified counterparts ($p < 0.001$), confirming that PLGA-PEG-Mal nanoparticles adhere well to the bladder mucosa by forming covalent linkages with thiol groups present in mucin layer of the bladder epithelium (Fig. 8). Such selective binding leads to increased urothelium cell uptake and potentially improved drug bioavailability within the bladder wall. The nanoparticles remained on the bladder mucosa even after 50 min of washing with a cumulative AU volume of 100 mL. This is in good agreement with our previous findings [28,29],

therefore the results of retention study confirm the mucoadhesive properties of maleimide-functionalised PLGA-PEG nanoparticles, which could also be used as potential mucoadhesive drug carriers in IDD to urinary bladder.

Previously we have introduced a novel quantitative method of evaluating and comparing the retention efficacy of liquid formulations on mucosal membranes through the use of WO_{50} values, which represent the volume of a biological fluid necessary to wash out 50 % of the mucoadhesive test material from a substrate [45]. In this study, we employed the same method and calculated WO_{50} values by analysing individual wash-off profiles for each nanoparticle suspensions and the results are presented in Table 1. By comparing these values for different PLGA-PEG nanoparticles used in this study, it is clear that $PLGA_{20K}$-PEG_{5K}-Mal have greater retention on lamb bladder mucosa (WO_{50} = 15 mL, R^2 = 1) compared to unmodified $PLGA_{20K}$-PEG_{5K} (WO_{50} = 5 mL, R^2 = 0.9872).

4. Conclusions

Four different types of PLGA-PEG nanoparticles were prepared and evaluated in this study for their physicochemical characteristics and retention on urinary bladder mucosa. The nanoparticles decorated with maleimide functional groups demonstrated greater retention on the bladder mucosa *in vitro* due to their ability to form covalent linkages with thiol groups of glycoproteins expressed on the bladder epithelial membrane. The biocompatibility of PEG-Mal was confirmed by SMIT assay experiments.

The development of mucoadhesive drug delivery systems that could improve drug residence in the bladder will clearly be beneficial for the treatment of bladder cancer. However, all existing strategies to develop mucoadhesive materials do not provide dosage forms that could selectively bind to cancer cells without adhesion to healthy epithelial cells. The development of systems that could target cancer cells in the bladder is one of the challenges for future research and development in this area.

The maleimide-functionalised PLGA-PEG mucoadhesive nanoparticles developed in this work could potentially be considered as a platform technology that could be used for drug delivery not only to the bladder but also to other mucosal routes of drug administration. Further research will be focused on biodegradation of these nanoparticles and studies of anticancer drugs encapsulation and release.

Acknowledgements

The authors gratefully acknowledge the British Council Newton – Al-Farabi Partnership Programme, the Researcher Links Post-Doctoral Mobility Grant (No. 216046068) for financial support and for providing 2-years postdoctoral fellowship for Dr D.B. Kaldybekov at the University of Reading. The Chemical Analysis Facility (University of Reading) is thanked for access to a fluorescence spectrophotometer and TEM. Dr S.K. Filippov acknowledges the financial support of U.S.–Czech Republic Fulbright Commission. P.C. Turner Abattoirs (Farnborough, UK) is also acknowledged for providing lamb urinary bladders for experiments.

Conflict of interest

The authors have no conflicts of interest to disclose.

Author contributions

The manuscript was written through contributions of all authors. All authors have given approval to the final version of the manuscript.

Appendix A. Supplementary material

Supplementary data associated with this article is available free of charge. It contains a standard curve used to determine the amount of encapsulated fluorescein in the PLGA-PEG nanoparticles (Fig. S1); detailed schematic illustration of SMIT test (Fig. S2) and the photographs of mucus production by *Arion lusitanicus* slugs in contact with test materials (Fig. S3).

Abbreviations

AU, artificial urine; BAC, benzalkonium chloride; BC, bladder cancer; D_2O, deuterium oxide; DLS, dynamic light scattering; DMSO, dimethyl sulfoxide; EE%, encapsulation efficiency; IDD, intravesical drug delivery; LC%, loading capacity; Mal, maleimide; MHA, 6-Maleimidohexanoic acid; MP%, mucus production; NPs, nanoparticles; PBS, phosphate buffered saline; PDI, polydispersity index; PEG, poly(ethylene glycol) methyl ether; PEG-Mal, methoxypolyethylene glycol maleimide; PLGA-PEG, poly(lactide-co-glycolide)-block-polyethylene glycol); SANS, small-angle neutron scattering; SMIT, slug mucosal irritation test; TEM, transmission electron microscopy; UA, uranyl acetate; WO_{50}, Wash Out 50%.

ORCID ID of authors

Daulet B. Kaldybekov: https://orcid.org/0000-0002-7191-5465

Vitaliy V. Khutoryanskiy: https://orcid.org/0000-0002-7221-2630

References

[1] V. V. Khutoryanskiy, Mucoadhesive materials and drug delivery systems, John Wiley & Sons, Ltd, Chichester, UK, 2014. doi:10.1002/9781118794203.

[2] G. Prosperi-Porta, S. Kedzior, B. Muirhead, H. Sheardown, Phenylboronic-acid-based polymeric micelles for mucoadhesive anterior segment ocular drug delivery, Biomacromolecules. 17 (2016) 1449–1457. doi:10.1021/acs.biomac.6b00054.

[3] B. Sarmento, A. Ribeiro, F. Veiga, D. Ferreira, R. Neufeld, Oral bioavailability of insulin contained in polysaccharide nanoparticles, Biomacromolecules. 8 (2007) 3054–3060. doi:10.1021/bm0703923.

[4] Y.G. Seo, D.W. Kim, W.H. Yeo, T. Ramasamy, Y.K. Oh, Y.J. Park, J.A. Kim, D.H. Oh, S.K. Ku, J.K. Kim, C.S. Yong, J.O. Kim, H.G. Choi, Docetaxel-loaded thermosensitive and bioadhesive

nanomicelles as a rectal drug delivery system for enhanced chemotherapeutic effect, Pharm. Res. 30 (2013) 1860–1870. doi:10.1007/s11095-013-1029-0.

[5] C.M. Caramella, S. Rossi, F. Ferrari, M.C. Bonferoni, G. Sandri, Mucoadhesive and thermogelling systems for vaginal drug delivery, Adv. Drug Deliv. Rev. 92 (2015) 39–52. doi:10.1016/j.addr.2015.02.001.

[6] C. Rieger, D. Kunhardt, A. Kaufmann, D. Schendel, D. Huebner, K. Erdmann, S. Propping, M.P. Wirth, B. Schwenzer, S. Fuessel, S. Hampel, Characterization of different carbon nanotubes for the development of a mucoadhesive drug delivery system for intravesical treatment of bladder cancer, Int. J. Pharm. 479 (2015) 357–363. doi:10.1016/j.ijpharm.2015.01.017.

[7] M. Hornof, W. Weyenberg, A. Ludwig, A. Bernkop-Schnürch, Mucoadhesive ocular insert based on thiolated poly(acrylic acid): Development and in vivo evaluation in humans, J. Control. Release. 89 (2003) 419–428. doi:10.1016/S0168-3659(03)00135-4.

[8] J.F. Fangueiro, F. Veiga, A.M. Silva, E.B. Souto, Ocular drug delivery – new strategies for targeting anterior and posterior segments of the eye, Curr. Pharm. Des. 22 (2016) 1135–1146. doi:http://dx.doi.org/10.2174/1381612822666151216145900.

[9] M. Kapoor, J.C. Cloyd, R.A. Siegel, A review of intranasal formulations for the treatment of seizure emergencies, J. Control. Release. 237 (2016) 147–159. doi:10.1016/j.jconrel.2016.07.001.

[10] L. Kozlovskaya, M. Abou-Kaoud, D. Stepensky, Quantitative analysis of drug delivery to the brain via nasal route, J. Control. Release. 189 (2014) 133–140. doi:10.1016/j.jconrel.2014.06.053.

[11] C. Mugabe, Y. Matsui, A.I. So, M.E. Gleave, J.H.E. Baker, A.I. Minchinton, I. Manisali, R. Liggins, D.E. Brooks, H.M. Burt, In vivo evaluation of mucoadhesive nanoparticulate docetaxel for intravesical treatment of non-muscle-invasive bladder cancer, Clin. Cancer Res. 17 (2011) 2788–2798. doi:10.1158/1078-0432.CCR-10-2981.

[12] R.R. De Araújo Pereira, M.L. Bruschi, Vaginal mucoadhesive drug delivery systems, Drug Dev. Ind. Pharm. 38 (2012) 643–652. doi:10.3109/03639045.2011.623355.

[13] O.M. Kolawole, W.M. Lau, H. Mostafid, V. V. Khutoryanskiy, Advances in intravesical drug delivery systems to treat bladder cancer, Int. J. Pharm. 532 (2017) 105–117. doi:10.1016/J.IJPHARM.2017.08.120.

[14] A.R. Mackie, F.M. Goycoolea, B. Menchicchi, C.M. Caramella, F. Saporito, S. Lee, K. Stephansen, I.S. Chronakis, M. Hiorth, M. Adamczak, M. Waldner, H. Mørck Nielsen, L. Marcelloni, Innovative methods and applications in mucoadhesion research, Macromol. Biosci. 17 (2017) 1600534. doi:10.1002/mabi.201600534.

[15] P. Tyagi, P.C. Wu, M. Chancellor, N. Yoshimura, L. Huang, Recent advances in intravesical drug/gene delivery, Mol. Pharm. 3 (2006) 369–379. doi:10.1021/mp060001j.

[16] S. GuhaSarkar, R. Banerjee, Intravesical drug delivery: Challenges, current status, opportunities and novel strategies, J. Control. Release. 148 (2010) 147–159. doi:10.1016/j.jconrel.2010.08.031.

[17] I.A. Sogias, A.C. Williams, V. V. Khutoryanskiy, Why is chitosan mucoadhesive?, Biomacromolecules. 9 (2008) 1837–1842. doi:10.1021/bm800276d.

[18] E. Bilensoy, C. Sarisozen, G. Esendağli, A.L. Doğan, Y. Aktaş, M. Şen, N.A. Mungan, Intravesical cationic nanoparticles of chitosan and polycaprolactone for the delivery of Mitomycin C to bladder tumors, Int. J. Pharm. 371 (2009) 170–176. doi:10.1016/j.ijpharm.2008.12.015.

[19] H.T. Ta, C.R. Dass, D.E. Dunstan, Injectable chitosan hydrogels for localised cancer therapy, J. Control. Release. 126 (2008) 205–216. doi:10.1016/j.jconrel.2007.11.018.

[20] I. Bravo-Osuna, M. Noiray, E. Briand, A.M. Woodward, P. Argüeso, I.T.M. Martínez, R. Herrero-Vanrell, G. Ponchel, Interfacial interaction between transmembrane ocular mucins and adhesive polymers and dendrimers analyzed by surface plasmon resonance, Pharm. Res. 29 (2012) 2329–2340. doi:10.1007/s11095-012-0761-1.

[21] M. Burjak, M. Bogataj, M. Velnar, I. Grabnar, A. Mrhar, The study of drug release from microspheres adhered on pig vesical mucosa, Int. J. Pharm. 224 (2001) 123–130. doi:10.1016/S0378-5173(01)00748-7.

[22] A. Bernkop-Schnürch, Thiomers: The next generation of mucoadhesive polymers, Adv. Drug Deliv. Rev. 57 (2005) 1569–1582. doi:10.1016/j.addr.2005.07.002.

[23] A. Bernkop-Schnürch, D. Guggi, Y. Pinter, Thiolated chitosans: Development and in vitro evaluation of a mucoadhesive, permeation enhancing oral drug delivery system, J. Control. Release. 94 (2004) 177–186. doi:10.1016/j.jconrel.2003.10.005.

[24] T. Schmitz, V. Grabovac, T.F. Palmberger, M.H. Hoffer, A. Bernkop-Schnürch, Synthesis and characterization of a chitosan-N-acetyl cysteine conjugate, Int. J. Pharm. 347 (2008) 79–85. doi:10.1016/j.ijpharm.2007.06.040.

[25] J. Iqbal, G. Shahnaz, S. Dünnhaupt, C. Müller, F. Hintzen, A. Bernkop-Schnürch, Preactivated thiomers as mucoadhesive polymers for drug delivery, Biomaterials. 33 (2012) 1528–1535. doi:10.1016/j.biomaterials.2011.10.021.

[26] J. Barthelmes, G. Perera, J. Hombach, S. Dünnhaupt, A. Bernkop-Schnürch, Development of a mucoadhesive nanoparticulate drug delivery system for a targeted drug release in the bladder, Int. J. Pharm. 416 (2011) 339–345. doi:10.1016/j.ijpharm.2011.06.033.

[27] N. Denora, A. Lopedota, M. Perrone, V. Laquintana, R.M. Iacobazzi, A. Milella, E. Fanizza, N. Depalo, A. Cutrignelli, A. Lopalco, M. Franco, Spray-dried mucoadhesives for intravesical drug delivery using N-acetylcysteine- and glutathione-glycol chitosan conjugates, Acta Biomater. 43 (2016) 170–184. doi:10.1016/j.actbio.2016.07.025.

[28] P. Tonglairoum, R.P. Brannigan, P. Opanasopit, V. V. Khutoryanskiy, Maleimide-bearing nanogels as novel mucoadhesive materials for drug delivery, J. Mater. Chem. B. 4 (2016) 6581–6587. doi:10.1039/C6TB02124G.

[29] D.B. Kaldybekov, P. Tonglairoum, P. Opanasopit, V. V. Khutoryanskiy, Mucoadhesive maleimide-functionalised liposomes for drug delivery to urinary bladder, Eur. J. Pharm. Sci. 111 (2018) 83–90. doi:10.1016/j.ejps.2017.09.039.

[30] Y. Shtenberg, M. Goldfeder, A. Schroeder, H. Bianco-Peled, Alginate modified with maleimide-

terminated PEG as drug carriers with enhanced mucoadhesion, Carbohydr. Polym. 175 (2017) 337–346. doi:10.1016/j.carbpol.2017.07.076.

[31] N. Sahatsapan, T. Rojanarata, T. Ngawhirunpat, P. Opanasopit, P. Tonglairoum, 6-Maleimidohexanoic acid-grafted chitosan: A new generation mucoadhesive polymer, Carbohydr. Polym. 202 (2018) 258–264. doi:https://doi.org/10.1016/j.carbpol.2018.08.119.

[32] Y. Xu, C.S. Kim, D.M. Saylor, D. Koo, Polymer degradation and drug delivery in PLGA-based drug–polymer applications: A review of experiments and theories, J. Biomed. Mater. Res. - Part B Appl. Biomater. 105 (2017) 1692–1716. doi:10.1002/jbm.b.33648.

[33] C. Jin, N. Qian, W. Zhao, W. Yang, L. Bai, H. Wu, M. Wang, W. Song, K. Dou, Improved therapeutic effect of DOX-PLGA-PEG micelles decorated with bivalent fragment HAb18 F(ab′)2for hepatocellular carcinoma, Biomacromolecules. 11 (2010) 2422–2431. doi:10.1021/bm1005992.

[34] K. Zhang, X. Tang, J. Zhang, W. Lu, X. Lin, Y. Zhang, B. Tian, H. Yang, H. He, PEG-PLGA copolymers: Their structure and structure-influenced drug delivery applications, J. Control. Release. 183 (2014) 77–86. doi:10.1016/j.jconrel.2014.03.026.

[35] U. Bazylińska, Rationally designed double emulsion process for co-encapsulation of hybrid cargo in stealth nanocarriers, Colloids Surfaces A Physicochem. Eng. Asp. 532 (2017) 476–482. doi:10.1016/j.colsurfa.2017.04.027.

[36] Y. Pei, M.F. Mohamed, M.N. Seleem, Y. Yeo, Particle engineering for intracellular delivery of vancomycin to methicillin-resistant Staphylococcus aureus (MRSA)-infected macrophages, J. Control. Release. 267 (2017) 133–143. doi:10.1016/j.jconrel.2017.08.007.

[37] A.S. Wadajkar, J.G. Dancy, N.B. Roberts, N.P. Connolly, D.K. Strickland, J.A. Winkles, G.F. Woodworth, A.J. Kim, Decreased non-specific adhesivity, receptor targeted (DART) nanoparticles exhibit improved dispersion, cellular uptake, and tumor retention in invasive gliomas, J. Control. Release. 267 (2017) 144–153. doi:10.1016/j.jconrel.2017.09.006.

643 [38] L. Zhang, Y. Shi, Y. Song, X. Sun, X. Zhang, K. Sun, Y. Li, The use of low molecular weight
644 protamine to enhance oral absorption of exenatide, Int. J. Pharm. 547 (2018) 265–273.
645 doi:https://doi.org/10.1016/j.ijpharm.2018.05.055.
646 [39] B. Zhang, P. Sai Lung, S. Zhao, Z. Chu, W. Chrzanowski, Q. Li, Shape dependent cytotoxicity of
647 PLGA-PEG nanoparticles on human cells, Sci. Rep. 7 (2017) 7315. doi:10.1038/s41598-017-
648 07588-9.
649 [40] A. Radulescu, N.K. Szekely, M.-S. Appavou, KWS-2: Small angle scattering diffractometer, J.
650 Large-Scale Res. Facil. JLSRF. 1 (2015) A29. doi:10.17815/jlsrf-1-27.
651 [41] I. Breßler, J. Kohlbrecher, A.F. Thünemann, SASfit : A tool for small-angle scattering data
652 analysis using a library of analytical expressions, J. Appl. Crystallogr. 48 (2015) 1587–1598.
653 doi:10.1107/S1600576715016544.
654 [42] J.S. Pedersen, M.C. Gerstenberg, The structure of P85 Pluronic block copolymer micelles
655 determined by small-angle neutron scattering, Colloids Surfaces A Physicochem. Eng. Asp. 213
656 (2003) 175–187. doi:10.1016/S0927-7757(02)00511-3.
657 [43] O. V. Khutoryanskaya, P.W.J. Morrison, S.K. Seilkhanov, M.N. Mussin, E.K. Ozhmukhametova,
658 T.K. Rakhypbekov, V. V. Khutoryanskiy, Hydrogen-bonded complexes and blends of
659 poly(acrylic acid) and methylcellulose: Nanoparticles and mucoadhesive films for ocular delivery
660 of riboflavin, Macromol. Biosci. 14 (2014) 225–234. doi:10.1002/mabi.201300313.
661 [44] S. Chutipongtanate, V. Thongboonkerd, Systematic comparisons of artificial urine formulas for in
662 vitro cellular study, Anal. Biochem. 402 (2010) 110–112. doi:10.1016/j.ab.2010.03.031.
663 [45] E.A. Mun, A.C. Williams, V. V. Khutoryanskiy, Adhesion of thiolated silica nanoparticles to
664 urinary bladder mucosa: Effects of PEGylation, thiol content and particle size, Int. J. Pharm. 512
665 (2016) 32–38. doi:10.1016/j.ijpharm.2016.08.026.
666 [46] A.I. Vogel, B.S. Furniss, Vogel’s textbook of practical organic chemistry, Longman, Harlow,
667 Essex, England, 1989. https://books.google.kz/books?id=2eQPAQAAMAAJ.

[47] B. Yang, J.P. Lowe, R. Schweins, K.J. Edler, Small angle neutron scattering studies on the internal structure of poly(lactide-co-glycolide)-block-poly(ethylene glycol) nanoparticles as drug delivery vehicles, Biomacromolecules. 16 (2015) 457–464. doi:10.1021/bm501519u.

[48] J.H. Lass, Advances in Corneal Research: Selected Transactions of the World Congress on the Cornea IV, Springer Science & Business Media, Boston, MA, 1998. https://books.google.kz/books?id=7wGH80U8tUIC.

[49] S. Bantle, M. Schmidt, W. Burchard, Simultaneous static and dynamic light scattering, Macromolecules. 15 (1982) 1604–1609. doi:10.1021/ma00234a028.

[50] W. Burchard, Static and dynamic light scattering from branched polymers and biopolymers, Light Scatt. from Polym. Adv. Polym. Sci. 48 (1983) 1–124. doi:10.1007/3-540-12030-0_1.

[51] W. Brown, Light scattering: Principles and development, Clarendon Press, Oxford, England, 1996. https://books.google.co.uk/books?id=RsNQGIlEbpwC.

[52] D. Gromadzki, S. Filippov, M. Netopilík, R. Makuška, A. Jigounov, J. Pleštil, J. Horský, P. Štěpánek, Combination of "living" nitroxide-mediated and photoiniferter-induced "grafting from" free-radical polymerizations: From branched copolymers to unimolecular micelles and microgels, Eur. Polym. J. 45 (2009) 1748–1758. doi:10.1016/j.eurpolymj.2009.02.022.

[53] M. Hruby, C. Konak, J. Kucka, M. Vetrik, S.K. Filippov, D. Vetvicka, H. Mackova, G. Karlsson, K. Edwards, B. Rihova, K. Ulbrich, Thermoresponsive, hydrolytically degradable polymer micelles intended for radionuclide delivery, Macromol. Biosci. 9 (2009) 1016–1027. doi:10.1002/mabi.200900083.

[54] T. Riley, C.R. Heald, S. Stolnik, M.C. Garnett, L. Illum, S.S. Davis, S.M. King, R.K. Heenan, S.C. Purkiss, R.J. Barlow, P.R. Gellert, C. Washington, Core−shell structure of PLA−PEG nanoparticles used for drug delivery, Langmuir. 19 (2003) 8428–8435. doi:10.1021/la020911h.

[55] M.J. Park, K. Char, Gelation of PEO−PLGA−PEO triblock copolymers induced by macroscopic phase separation, Langmuir. 20 (2004) 2456–2465. doi:10.1021/la035573e.

[56] N.K. Khorshid, K. Zhu, K.D. Knudsen, S. Bekhradnia, S.A. Sande, B. Nyström, Novel structural changes during temperature-induced self-assembling and gelation of PLGA-PEG-PLGA triblock copolymer in aqueous solutions, Macromol. Biosci. 16 (2016) 1838–1852. doi:10.1002/mabi.201600277.

[57] T. Maeda, M. Kitagawa, A. Hotta, S. Koizumi, Thermo-responsive nanocomposite hydrogels based on PEG-b-PLGA diblock copolymer and laponite, Polymers (Basel). 11 (2019) 250. doi:10.3390/polym11020250.

[58] E. Adriaens, J.P. Remon, Gastropods as an evaluation tool for screening the irritating potency of absorption enhancers and drugs, Pharm. Res. 16 (1999) 1240–1244. doi:10.1023/A:1014801714590.

[59] E. Adriaens, K. Dierckens, T.G.M. Bauters, H.J. Nelis, F. Van Goethem, P. Vanparys, J.P. Remon, The mucosal toxicity of different benzalkonium chloride analogues evaluated with an alternative test using slugs, Pharm. Res. 18 (2001) 937–942. doi:10.1023/A:1010928025753.

[60] J. Lenoir, C. Bachert, J.P. Remon, E. Adriaens, The Slug Mucosal Irritation (SMI) assay: A tool for the evaluation of nasal discomfort, Toxicol. Vitr. 27 (2013) 1954–1961. doi:10.1016/j.tiv.2013.06.018.

[61] O. V. Khutoryanskaya, Z.A. Mayeva, G.A. Mun, V. V. Khutoryanskiy, Designing temperature-responsive biocompatible copolymers and hydrogels based on 2-hydroxyethyl(meth)acrylates, Biomacromolecules. 9 (2008) 3353–3361. doi:10.1021/bm8006242.

GRAPHICAL ABSTRACT

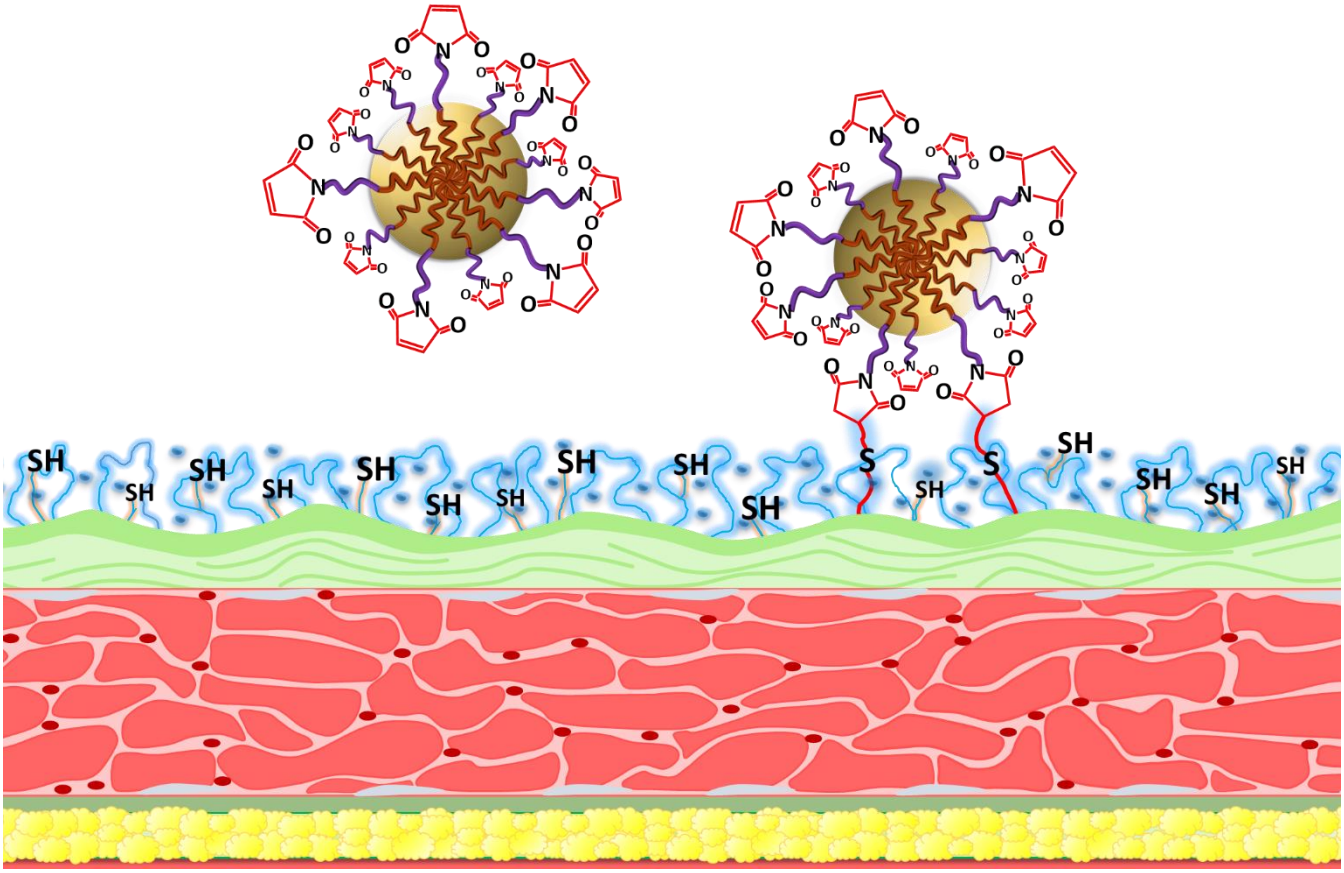

Schematic illustration depicting the mechanism of enhanced mucoadhesion of PLGA-PEG-Mal nanoparticles on urinary bladder mucosa.

FIGURES WITH CAPTIONS

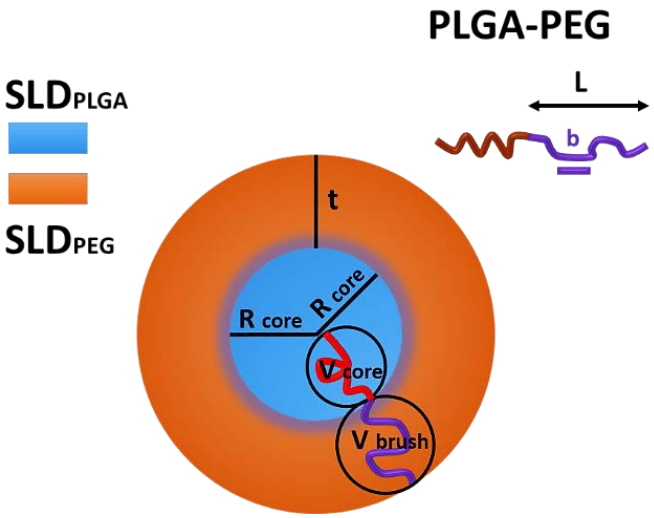

Fig. 1. The model used for the fitting of experimental SANS data.

(single column fitting image)

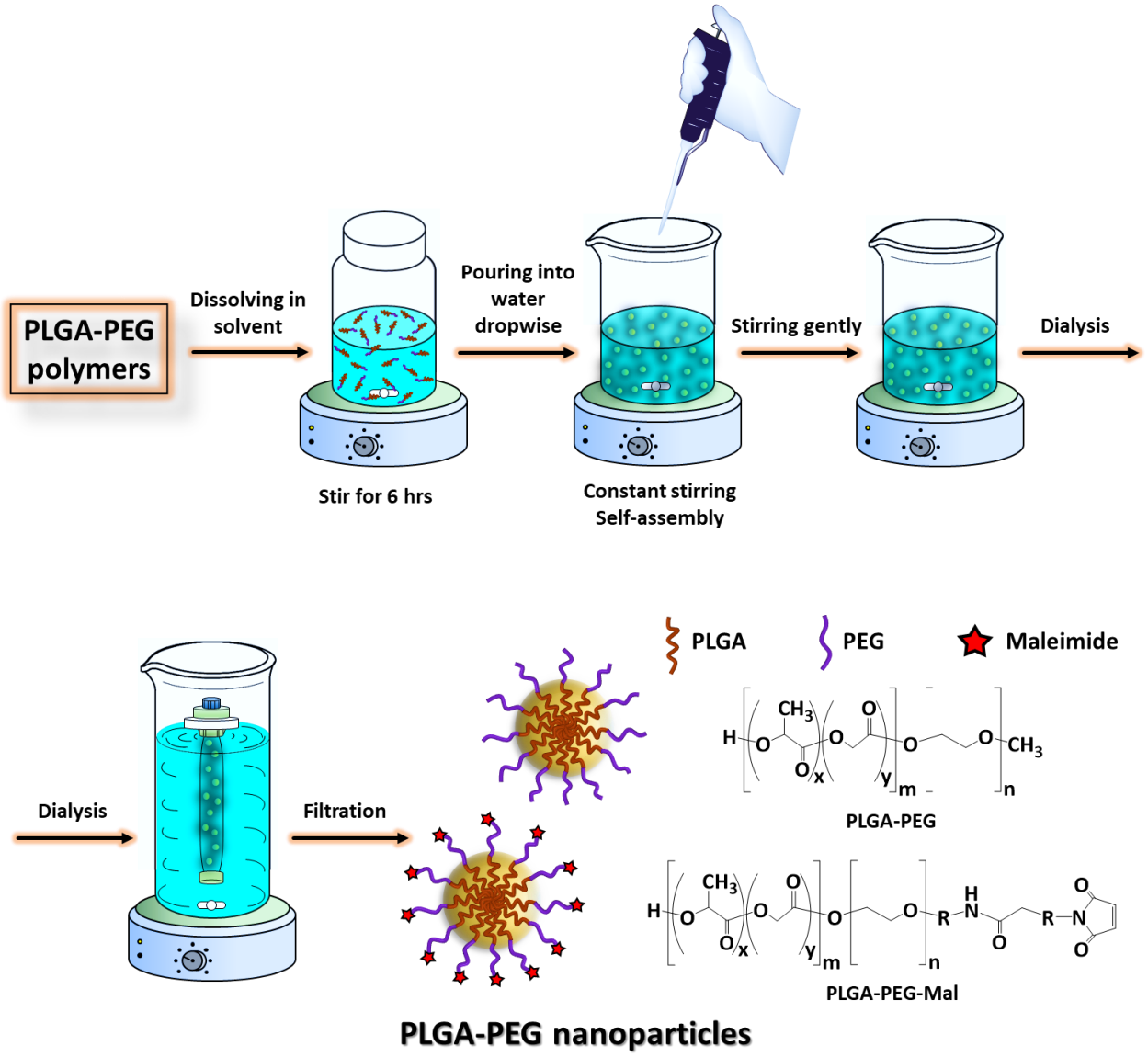

723

724 **Fig. 2.** Illustrative diagram depicting the preparation of PLGA-PEG nanoparticles with maleimide-

725 functionalised surface.

726 (2-column fitting image)

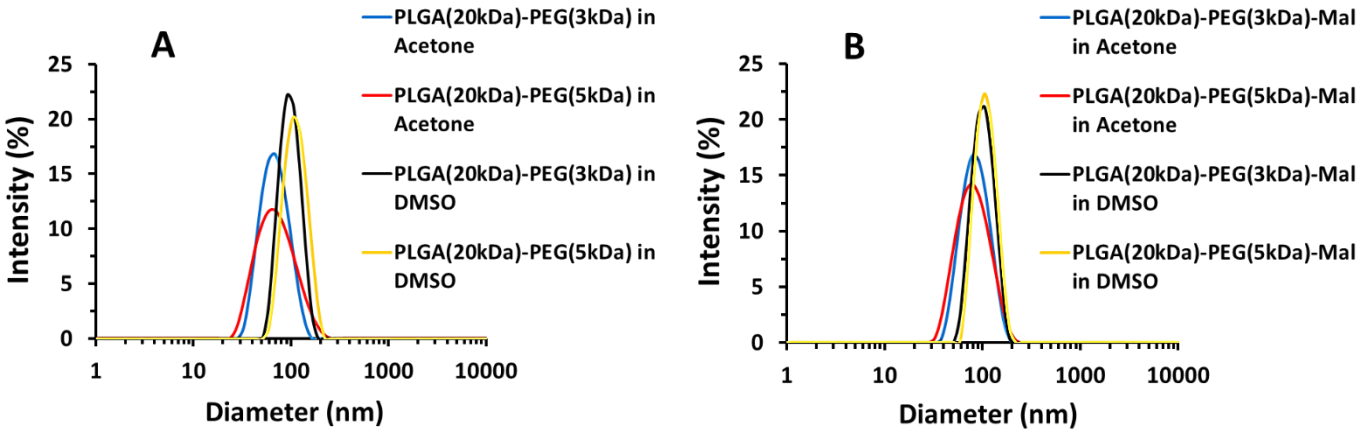

Fig. 3. Size distribution of PLGA-PEG (A) and PLGA-PEG-Mal (B) nanoparticles dissolved and precipitated from acetone and DMSO as determined by DLS.

(2-column fitting image)

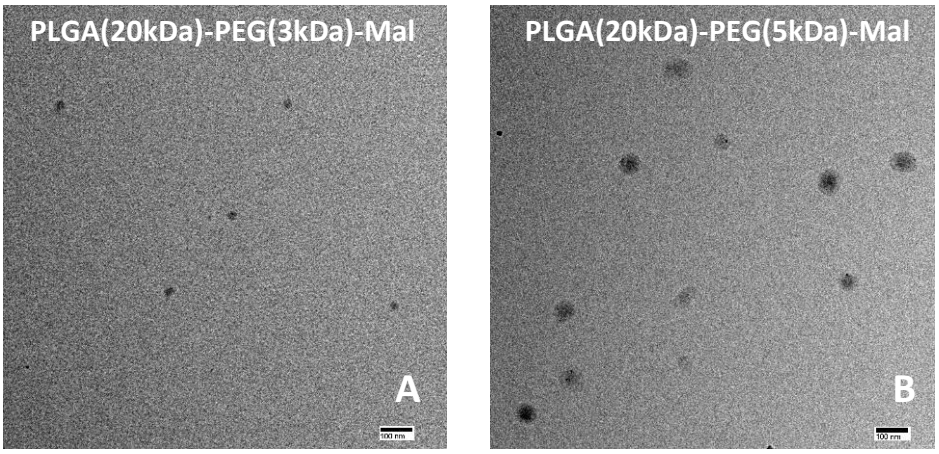

731

732 **Fig. 4.** TEM microphotographs of PLGA-PEG-Mal NPs dissolved and precipitated from acetone (A) and

733 DMSO (B). Scale bars are 100 nm.

734 (single column fitting image)

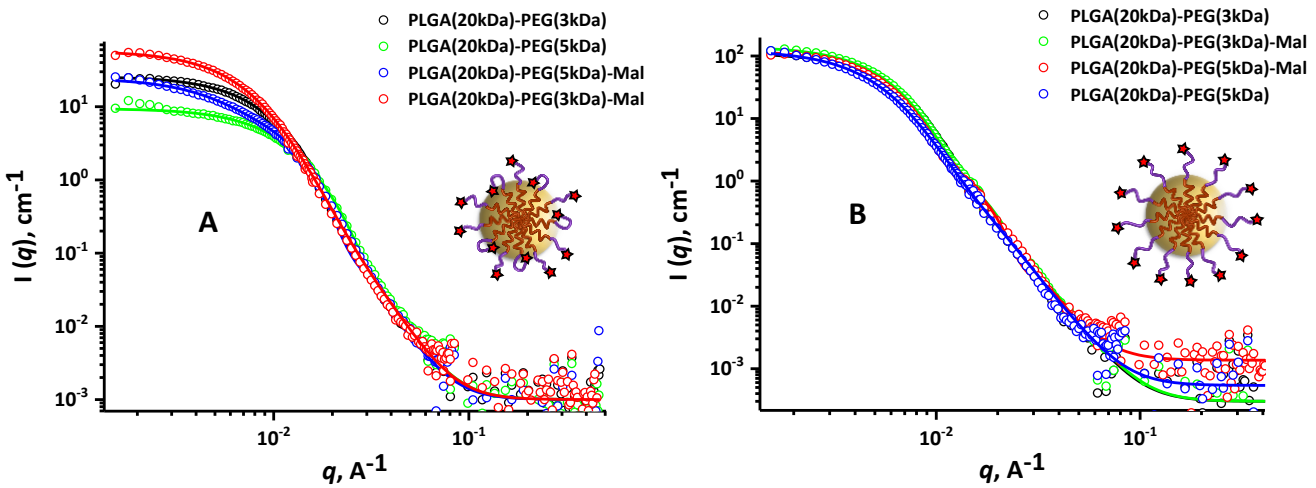

735

736 **Fig. 5.** SANS curves for PLGA-PEG nanoparticles dissolved and precipitated from acetone (A) and

737 DMSO (B). Solid line is a fitting curve. Inserts: Proposed structures of nanoparticles.

738 (2-column fitting image)

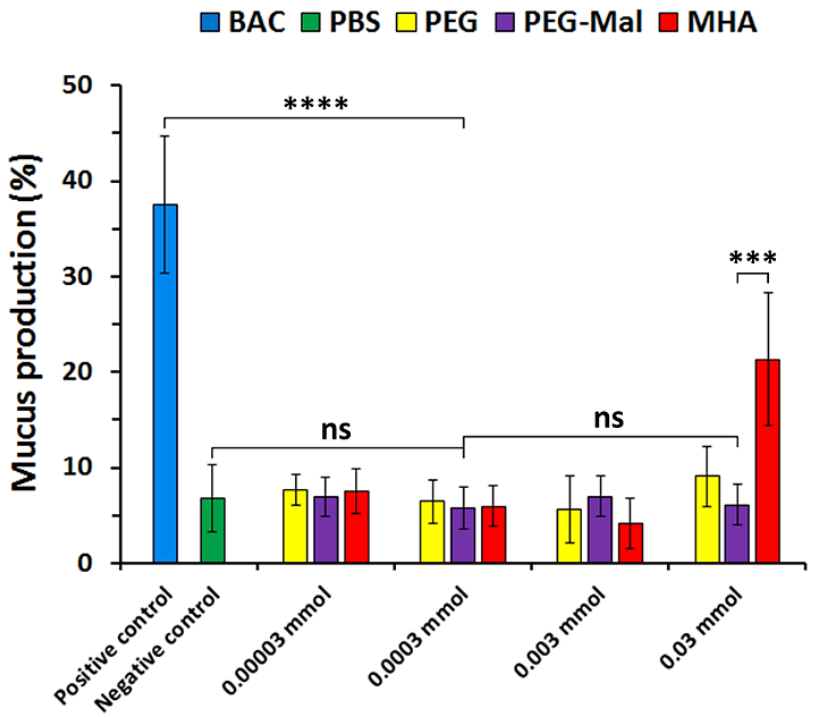

739

740 **Fig. 6.** Mucus production by *Arion lusitanicus* slugs in response to 60 min exposure to PEG, PEG-Mal
741 and MHA as well as positive (benzalkonium chloride – BAC) and negative (phosphate buffered saline –
742 PBS) controls. Data are expressed as mean ± standard deviation (n = 7). Statistically significant
743 differences are given as: **** – $p < 0.0001$; *** – $p < 0.001$; ns – no significance.

744 (single column fitting image)

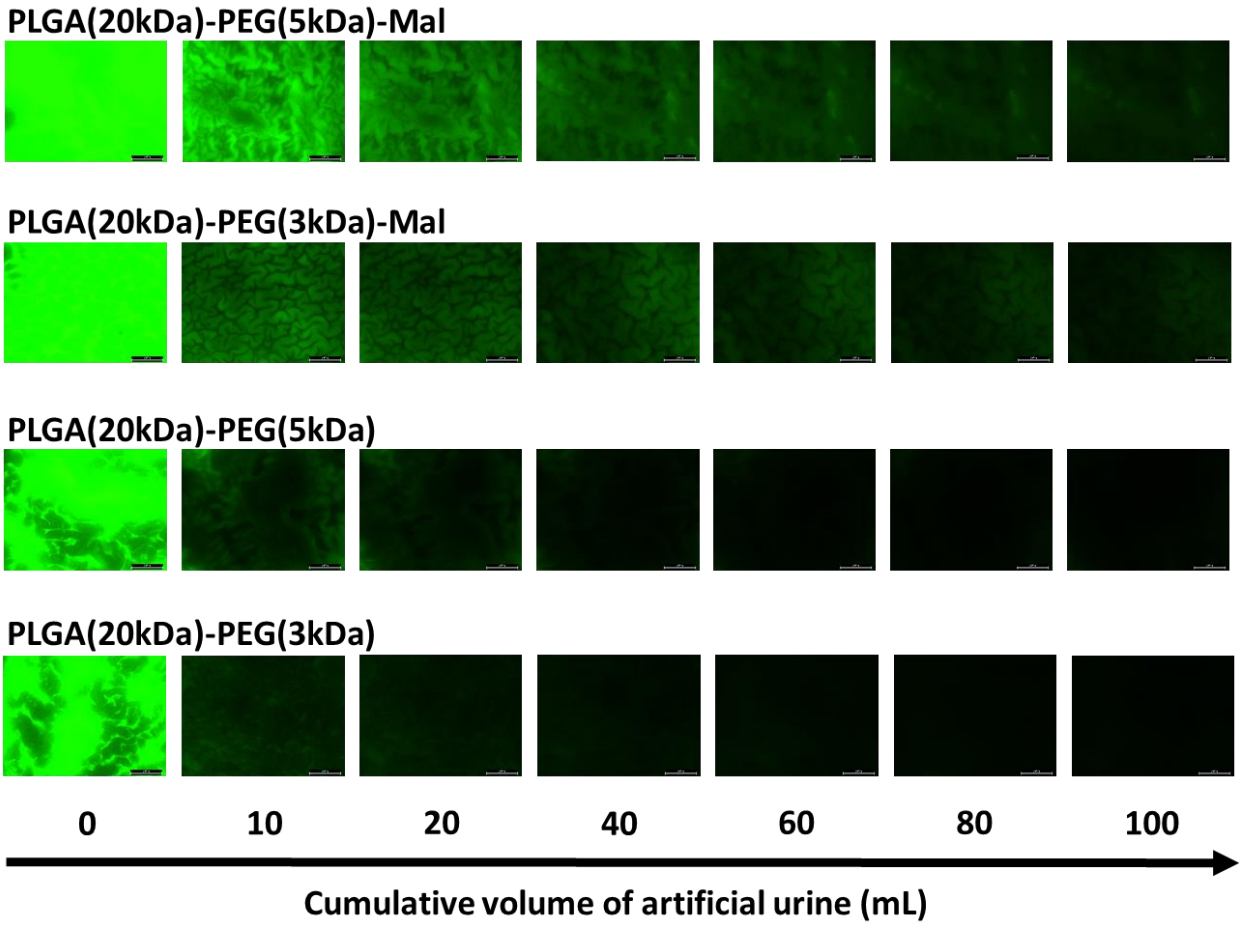

745

746 **Fig. 7.** Exemplar fluorescence images showing retention of PLGA-PEG nanoparticles on lamb urinary

747 bladder mucosa washed with different volumes of AU. Scale bars are 2 mm.

748 (2-column fitting image)

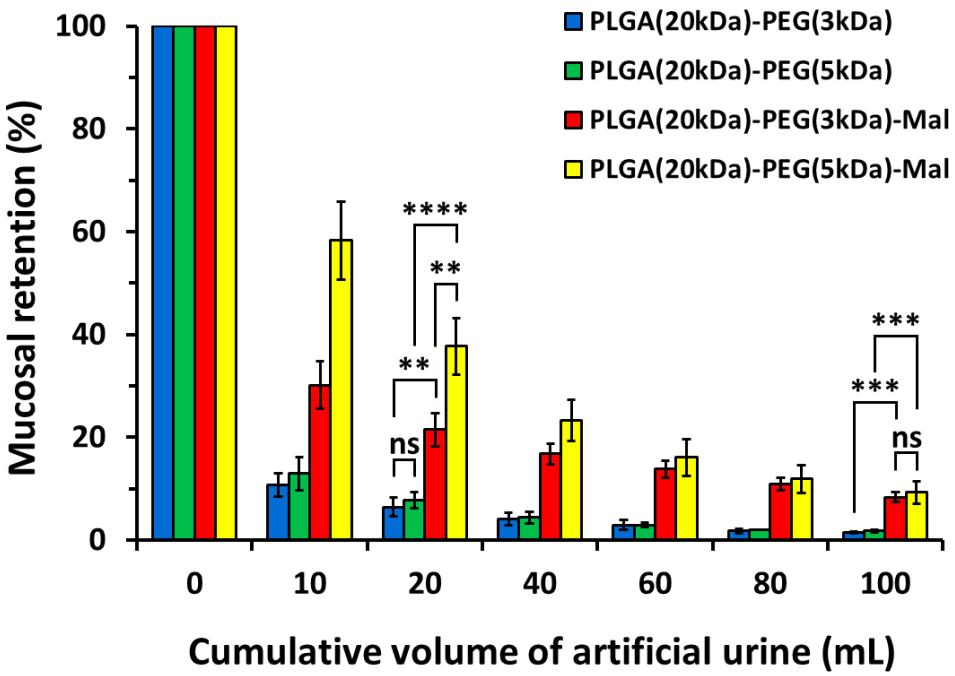

749

750 **Fig. 8.** Percentage retention of PLGA-PEG nanoparticles on lamb urinary bladder mucosa after irrigating
751 with different volumes of AU solution. Data are expressed as mean ± standard deviation (n = 3).
752 Statistically significant differences are given as: **** – $p < 0.0001$; *** – $p < 0.001$; ** – $p < 0.01$; ns
753 – no significance.

754 (single column fitting image)

TABLES WITH CAPTIONS

Table 1. Physicochemical characteristics of PLGA-PEG nanoparticles.

Formulation	Solvent used in NPs preparation	Mean diameter (nm)	PDI	Zeta-potential (mV)	EE%	LC%	WO_{50} (mL)*
$PLGA_{20K}$-PEG_{3K}	DMSO	94 ± 1	0.048	–20.8 ± 0.5	62.7 ± 3.6	3.1 ± 0.2	4; (R^2 = 0.9860)
$PLGA_{20K}$-PEG_{5K}		105 ± 1	0.070	–21.6 ± 0.4	63.8 ± 6.9	3.2 ± 0.4	5; (R^2 = 0.9872)
$PLGA_{20K}$-PEG_{3K}-Mal		98 ± 1	0.060	–17.7 ± 0.6	60.0 ± 4.2	3.0 ± 0.2	6; (R^2 = 0.9931)
$PLGA_{20K}$-PEG_{5K}-Mal		104 ± 1	0.067	–12.2 ± 0.5	55.0 ± 5.8	3.0 ± 0.3	15; (R^2 = 1)
$PLGA_{20K}$-PEG_{3K}	Acetone	64 ± 1	0.110	–8.1 ± 0.7	N/A	N/A	N/A
$PLGA_{20K}$-PEG_{5K}		68 ± 1	0.248	–5.2 ± 0.6	N/A	N/A	N/A
$PLGA_{20K}$-PEG_{3K}-Mal		80 ± 1	0.094	–16.5 ± 0.6	N/A	N/A	N/A
$PLGA_{20K}$-PEG_{5K}-Mal		81 ± 1	0.206	–10.8 ± 0.8	N/A	N/A	N/A

DMSO, dimethyl sulfoxide; PLGA-PEG, poly(lactide-*co*-glycolide)-*block*-polyethylene glycol); Mal, maleimide; PDI, polydispersity index; EE%, encapsulation efficiency; LC%, loading capacity; WO_{50}, Wash Out 50% profile is a volume of artificial urine required to wash out 50% liquid formulation; N/A, not applicable. *Polynomial fitting (5th order) was used to quantify WO_{50} values. Results are given as mean ± standard deviation (n =3).

(2-column fitting table)

Table 2. Comparison of structural parameters obtained from samples PLGA-PEG nanoparticles in D_2O

Formulation	Solvent used in NPs preparation	R_g (nm)	R_g/R_h	R_{core} (nm)	σ	R_{gchain} (nm)
$PLGA_{20K}$-PEG_{3K}	DMSO	35.7 ± 1.4	0.76	14.8 ± 0.1	0.43	12.0 ± 0.1
$PLGA_{20K}$-PEG_{5K}		40.8 ± 1.5	0.78	15.4 ± 0.2	0.63	12.1 ± 0.3
$PLGA_{20K}$-PEG_{3K}-Mal		35.7 ± 0.9	0.73	14.6 ± 0.1	0.31	14.4 ± 0.2
$PLGA_{20K}$-PEG_{5K}-Mal		35.5 ± 0.7	0.68	15.8 ± 0.2	0.20	16.7 ± 0.3
$PLGA_{20K}$-PEG_{3K}	Acetone	21.0 ± 0.8	0.66	10.2 ± 0.2	0.33	6.9 ± 0.1
$PLGA_{20K}$-PEG_{5K}		36.0 ± 0.5	1.06	12.0 ± 0.2	0.21	8.6 ± 0.1
$PLGA_{20K}$-PEG_{3K}-Mal		30.0 ± 1.0	0.75	12.8 ± 0.1	0.50	4.1 ± 0.2
$PLGA_{20K}$-PEG_{5K}-Mal		33.0 ± 2.0	0.81	12.0 ± 0.1	0.24	8.3 ± 0.1

DMSO, dimethyl sulfoxide; PLGA-PEG, poly(lactide-*co*-glycolide)-*block*-polyethylene glycol); Mal, maleimide; R_g, overall gyration radius of a nanoparticle; R_{core}, core radius; σ, polydispersity parameter; R_{gchain}, gyration radius of a polymer chain in the corona.

(single column fitting table)